NASA-CR-198595

INTERIM
IN-35-CR
OCIT
49942
P- 55

ANNUAL RESEARCH TECHNICAL REPORT ON STUDY OF DEVELOPMENT AND UTILIZATION OF A MULTIPURPOSE ATMOSPHERIC CORROSION SENSOR

NASA GRANT #NAG 10-0127

COLLEGE OF ENGINEERING
SOUTHERN UNIVERSITY
BATON ROUGE, LOUISIANA 70813

December, 1994

RAVINDER M. DIWAN, Ph.D.
PROFESSOR AND PRINCIPAL INVESTIGATOR

A. RAMAN, Ph.D.
ADJUNCT PROFESSOR AND CO-PRINCIPAL INVESTIGATOR

P.K. BHATTACHARYA, Ph.D.
ASSOCIATE PROFESSOR AND CO-PRINCIPAL INVESTIGATOR

SUBMITTED TO:

NASA KENNEDY SPACE CENTER
FLORIDA 32899

ANNUAL RESEARCH TECHNICAL REPORT

ON STUDY OF DEVELOPMENT AND UTILIZATION

OF A MULTIPURPOSE ATMOSPHERIC CORROSION SENSOR

NASA GRANT #NAG 10-0127

COLLEGE OF ENGINEERING
SOUTHERN UNIVERSITY
BATON ROUGE, LOUISIANA 70813

December, 1994

RAVINDER M. DIWAN, Ph.D.
PROFESSOR AND PRINCIPAL INVESTIGATOR

A. RAMAN, Ph.D.
ADJUNCT PROFESSOR AND CO-PRINCIPAL INVESTIGATOR

P.K. BHATTACHARYA, Ph.D.
ASSOCIATE PROFESSOR AND CO-PRINCIPAL INVESTIGATOR

SUBMITTED TO:

NASA KENNEDY SPACE CENTER
FLORIDA 32899

ANNUAL RESEARCH TECHNICAL REPORT

ON STUDY OF DEVELOPMENT AND UTILIZATION

OF A MULTIPURPOSE ATMOSPHERIC CORROSION SENSOR

NASA GRANT #NAG 10-0127

COLLEGE OF ENGINEERING
SOUTHERN UNIVERSITY
BATON ROUGE, LOUISIANA 70813

December, 1994

RAVINDER M. DIWAN, Ph.D.
PROFESSOR AND PRINCIPAL INVESTIGATOR

A. RAMAN, Ph.D.
ADJUNCT PROFESSOR AND CO-PRINCIPAL INVESTIGATOR

P.K. BHATTACHARYA, Ph.D.
ASSOCIATE PROFESSOR AND CO-PRINCIPAL INVESTIGATOR

SUBMITTED TO:

NASA KENNEDY SPACE CENTER
FLORIDA 32899

FOREWORD

The enclosed annual research technical report work has been carried out under NASA Grant # NAG 10-0127. The authors conducted a thorough review of the state of the art methods in atmospheric corrosion detection and a study and evaluation of development of a multipurpose atmospheric corrosion sensor. This research has been supported by NASA Kennedy Space Center, Florida. Dr. Rupert Lee, DM-MSL-22 served as the Technical Officer and Coordinator of the research project, with Mr. David Makufka and Ms. Joyce Beeson, OP-MSO-A as the Administrative Coordinators for this research project.

In addition to this annual research technical report , interim progress reports have been submitted periodically every three months on this project and a state of the art in atmospheric corrosion detection review report has been also submitted to Materials Science Laboratory, Kennedy Space Center.

Annual Research Technical Report Submitted:

Ravinder M. Diwan, Ph.D.
Professor and Principal Investigator
Southern University
Baton Rouge, LA 70813

December, 1994

ACKNOWLEDGMENT

The authors express their sincere gratitude and appreciation for the financial assistance provided through the NASA, Kennedy Space Center, Florida under Grant # NAG 10-0127. Appreciation is expressed to Dr. Rupert Lee of the Materials Science Laboratory, Kennedy Space Center, who served as the Technical Officer and Coordinator for this project and provided valuable collaborative technical support. Mr. David Makufka and Ms. Joyce Beeson of Kennedy Space Center, served as the Administrative Coordinators for this research project. Special thanks are expressed to them for their administrative support of this project.

TABLE OF CONTENTS

1.0 INTRODUCTION

There has been a critical need for analyzing the several aspects of atmospheric corrosion and for development of atmospheric corrosion microsensors. This project has been carried out in collaboration with the Materials Science Laboratory of NASA Kennedy Space Center, Florida. The project work has involved the following activities:

a) making of multielectrode corrosion monitors on dielectric substrates,
b) testing them in the laboratory for functional characteristics,
c) preparing a report on the state of the art of atmospheric corrosion sensor development around world, and
d) corrosion testing of electrochemical changes of sensor specimens and related fog testing.

The studies included work on the subject of development and utilization of a multipurpose atmospheric corrosion sensor and this report is the annual report on work carried out on this referenced research project. This has included studies on the development of sensors of two designs, stage I and stage II, and with glass and alumina substrate, experimentation and development and characterization of the coating uniformity, aspects of corrosion monitoring, literature search on the corrosion sensors and their development. A state of the art report on atmospheric corrosion sensor development was prepared and submitted (Reference R1). This project has involved the work and research efforts of Principal Investigator Dr. R. Diwan, and Co-principal Investigators Dr. P.K. Bhattacharya, and Dr. A. Raman. The experimental techniques are under development and being fine tuned and the research team has included the involvement and training of graduate students in Materials Program Mr. Manoj Chabbra, and Mr. Wensen Li and undergraduate engineering students Mr. Ali Darwish, Miss Felesha Robertson, Miss Lorann Jones and Mr. Chin-siung Teo.

R1. R. Diwan, A. Raman and P.K. Bhattacharya; Review Report on " State of the Art in Atmospheric Corrosion Detection", Submitted to NASA Kennedy Space Center, September, 1994.

The microsensor electrode experimental work on fabrication and corrosion testing is continuing and a proposal is under consideration for a continued further research in this area for three years as per the needs of NASA Kennedy Space Center.

2.0 APPROACH ON MICROSENSOR DESIGN CHARACTERISTICS

The principle of corrosion sensing calls for electrochemical evaluation of suitable thin film (TF) electrodes deposited on a dielectric substrate and exposed to the corrosive environment. The corrosion causing parameters can be evaluated with sensitive elements such as iron, aluminum, zinc, etc. Thin films of one or two different elements, either alone or in galvanic coupling can be exposed. Corrosion would occur due to moisture condensing on the elements along with any contaminants. The metallic film would corrode at a certain rate, proportional to the corrosion current developed by the metal being subjected to a specific potential, characteristic of the metal and the variables of the corroding environment, such as pH, ion concentration in the condensate, temperature, etc. Thus at a given site, under specific, nearly uniform atmospheric conditions, the corrosion potential of the metallic film and the corrosion current passing through it subjecting it to corrode would be of interest. These would vary, especially the current, if corroding conditions become severe, say due to sudden outbursts of pollutants into the atmosphere.

The corrosion potentials and the corrosion currents are to be determined using linear polarization and Tafel extrapolation techniques of electrochemistry. These are well known and described in standard textbooks on electrochemistry.

When two corrodible metals located on the same substrate are connected to each other and exposed to the corrosive atmosphere, one of them would corrode while the other would resist corrosion. This is from the principles of galvanic corrosion.

In our attempts at developing the atmospheric corrosion sensors (ACS) we have chosen iron and aluminum as the two corrodible metal electrodes, for the alloys of these elements are the most utilized structural materials in the atmosphere. To be able to perform the electrochemical tests, gold or 60% gold-40% palladium alloy film is used as the counter electrode and a silver thin film electrode suitably processed into a reference electrode would serve as the reference to read the potentials of the corroding metals.

In the corrosion experiments the open circuit corrosion potential will be first determined using the silver reference electrode. The corroding film electrode will then be connected to the gold film electrode and the potential varied in slow enough steps from 20 to 50 millivolt below the corrosion potential to about 20 millivolt or close to it above the corrosion potential. Such polarization of the corroding electrode film through use of a suitable function generator and d.c. potential imposition is required. The current is continuously monitored during the polarization process.

From the anodic polarization data, linear polarization resistance, the anodic and cathodic Tafel slopes are determined. These are then utilized in the Stern-Geary equation to determine the corrosion current.

The electrochemical testing of corrosion with these film electrodes would thus allow not only the determination of the corrosion current, but also enable abnormal-corrosion sensing through indications of sudden variations in corrosion currents. The periods of wetness when the metals are prone to maximum corrosion would also be automatically recorded.

3.0 DEVELOPMENT OF FILM DEPOSITION TECHNIQUES

The development of prototype atmospheric corrosion sensors can be generalized as fabrication of multiple thin film structures over an insulating and chemically inert slab acting as a substrate for the film components. The substrate is an important part of the sensor circuit and a base material which should not change during the life of the sensor. Ideally the base of the sensor should be optically plane, non porous, and dust free surface which can be packaged comfortably. However, actual properties of available substrates do influence the performance and cost of the resultant sensors. A perfect substrate should have:

1. A perfectly smooth chemically homogenous surface to permit growth of thin, defect free films.

2. A temperature coefficient of expansion that is identical to that of the films deposited so as to minimize peeling off due to mechanical stress in the films.

3. High mechanical strength and thermal shock resistance to enable the substrate to stand practical conditions and rigors of processing. This would make them stronger and perfect to tolerate thermal warping or expansion.

4. Inertness to chemicals used in circuit processing and corrosion atmosphere.

5. High electrical resistance and low power dissipation factor.

6. Low cost.

7. Uniform physical properties and standard dimensions that suit the size of the sensor.

Most commonly used substrate materials include various glasses, alumina, beryllia, sapphire, boron nitride, silicon, and spinels. Silicon must be coated with a dielectric film which is usually 5000Å to 10,000 Å of thermally grown SiO_2 or spin on glass. Both types of glasses (alumino or borosilicate glasses) are next in good smoothness.

One can use dielectric film coatings over normal silicon substrates to achieve chemical inertness and corrosion protection employing a planar process like diffusion or gettering of impurities, but it adds to its cost and inconvenience due to addition of more number of process steps. For our experiments, with the first set of sensors called stage I sensors, 1/4" thick glass slabs of 1" x 1.5" size were used . Then we switched to the most commonly used substrate material called sintered alumina because of its high thermal conductivity, good resistance to chemical attack and good mechanical rigidity. These are called stage II sensors. Details about these designs would be examined later. Alumina being a ceramic substrate is usually composed of sintered granules, thus its surface finish and porosity are not as good as those of glass or the single crystal Si substrates. Just to enable one to achieve the required characteristics of the substrate we can use the following methods (a) synthesis, (b) thin film epitaxy of suitable resistivity polysilicon, (c) oxides (d) nitrides (e) carbides and (f) silicides. Since these are prepared by chemical vapor deposition methods and involve more advanced process technologies in semiconductor processing, we have selected pyrosynthesis as a process to get alumina. However, it may in some cases be a preferentially deposited film over insulating subrstrate like glass or a polyimide or a film deposited over a preferentially doped substrate, which is not under direct control of the involved process when using chemical vapor deposition. In the case of crystalline substrates like (100) silicon we may come across orientation dependence of defects. Such effects can be used for processing of silicon embedded sensors, but are not found very attractive from applications point of view. The variations in thermal conductivity [R2] of various substrates are shown in figure 1.

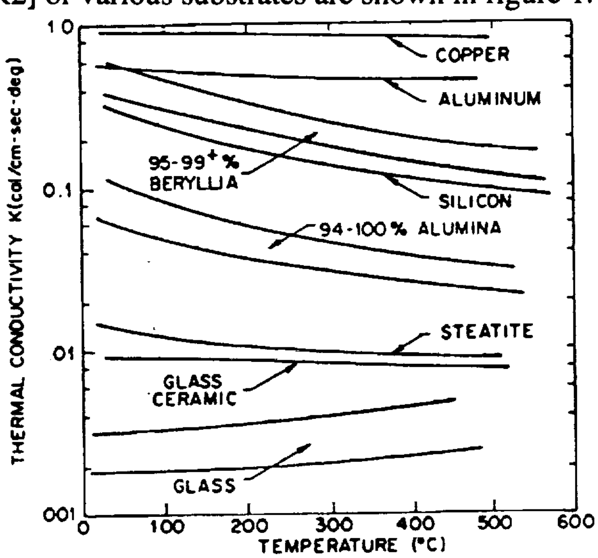

FIGURE 1: Thermal conductivity of various substrate materials substrates.

In our experimentation and coatings of the film structures, it was not found necessary to improve the surface finish or use costly glazed substrates. Figures 2 (i) and 2 (ii) show an Alpha -Step 200 (Tencor Profiler) stylus tracing of the substrate surface on smooth and spotchy sides. These roughness were in the order of 5000 Å for the smooth face to about 10,000 Å for the spotchy face. Figure 2(iii) shows meaning of commonly used definitions for the three component terms called the roughness, waviness and flatness shown as (b), (c) and (d), and (a) the whole track. In order to compare these with our samples, typical values of these parameters for standard substrates are shown in table I. These tables have been obtained from typical values obtained as a result of great deal of research and in the field of materials engineering.

TABLE I
Substrate Roughness and Flatness

Substrate Material	Roughness	Flatness
Soda-Lime Glass	< 250Å	20 μm/cm
Corning Code 7059 Glass	< 250 Å	40 μm/cm
Polished Sapphire	< 250 Å	< 1 μm/cm
Polished 99.94% Alumina (ultrafine grain)	≈ 250 Å	< 0.1 μm/cm
As Fired 99.5% Alumina (fine grain)	≈ 10,000 Å	50 μm/cm
Glazed Alumina	< 250 Å	50 μm/cm

We have used physical vapor deposition to achieve vacuum deposition, and employed evaporation and sputtering processes in particular. Hence the coating materials, which are metals for our sensors, are passed into a vapor transport phase by physical mechanisms like Joule evaporation, sputtering and electron or ion bombardment. Since many of the metals like Al have a native oxide which frequently etch very slowly and preferentially and can not be removed unless etched chemically selectively, giving a rough etching surface, we have ignored Al-Cu or Al-Si alloys which can perhaps solve these issues. One of the chief causes behind such decisions are to maintain chemical purity of the corroding electrodes. In this report no attempt is made to give a complete discussion of all the technologies but certain aspects would be highlighted that are of particular importance in sensor fabrication. For plasma deposition, a modified Reinberg [R3] design of sputtering reactor, with outward radial flow type plasma system(from Ted Pella Inc.) has been obtained and is in use. For inertness and safety consideration use of inert perflouropolythelene pump fluids are the best choice and a similar fluid has been selected for the vacuum system. No special film property measurement techniques were used. For measuring stoichiometry Rutherford Backscattering, Auger Electron Spectroscopy could be used to assess surface doping by corrosion. Hydrogen content can be evaluated by infra-red spectroscopy and nuclear reaction analysis, whereas refractive index changes can be measured by using ellipsometry and interference effects. These can be added to estimate etch rate using stylus step height measurement. Interface stress can be measured by induced curvature of substrate using optical reflection, leverage or X-ray measurement methods. Adhesion of the electrode films can be measured by ramped pull to failure, scribing and saw cutting techniques. Conformality can be detected using scanning electron microscope whereas pinhole density can be made using the latter or by employing a chemical or electrochemical etch mask followed by optical microscopy. For our purposes stress is a film property which mainly effects our investigation and is currently attracting much attention elsewhere.

The effects of stress are known to be dependent on the nature of the substrate, in terms both of film nucleation effects and of mismatch of thermal expansion coefficients, as well as deposition conditions. We have thus selected alumina as our high tensile stress substrate enabling good film/substrate adhesion and needed to prevent film peeling. Glass did not show such properties for all types of electrode films used.

R2. A.R. Glaser and G.E. Subak-Sharpe, "Integrated circuit Engineering," 2nd Edition, Addison-Wesley Publishing Co., Reading, (1970), p.350.

R3. G. E. McGuire, "Semiconductor Materials and Process Technology Handbook", Noyes Publications, New Jersey, (1988), p.364.

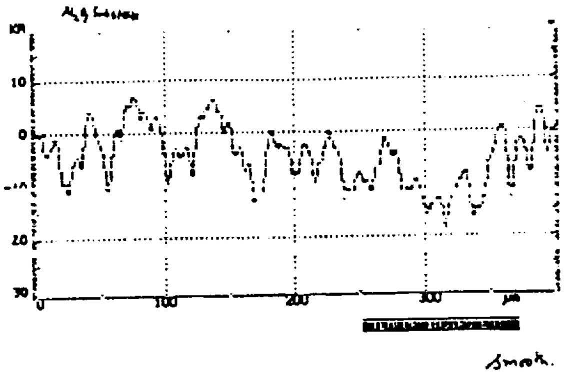

Figure 2(i) Al_2O_3 substrate Tencor profile showing smooth substrate surface.

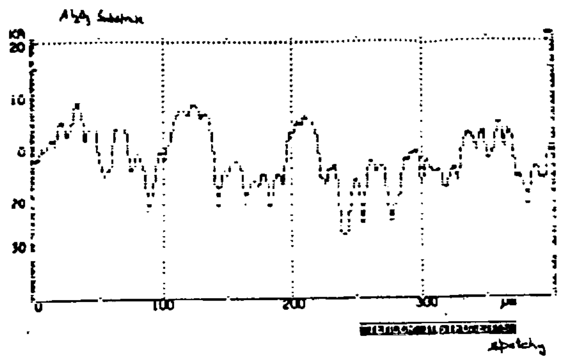

Figure 2(ii) Al_2O_3 substrate Tencor profile showing spotchy substrate surface.

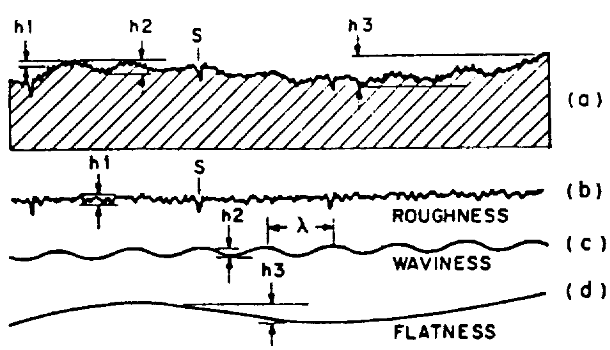

Figure 2(iii) Substrate surface finish. (a) Stylus tracing of surface; (b) roughness; (c) waviness; (d) flatness.

3.1. EVAPORATION TECHNIQUES

Evaporation was conducted in a vacuum environment at a base (initial) pressure in the range of 10^{-6} to 10^{-5} Torr in an evaporator such as that shown in the figure 3.

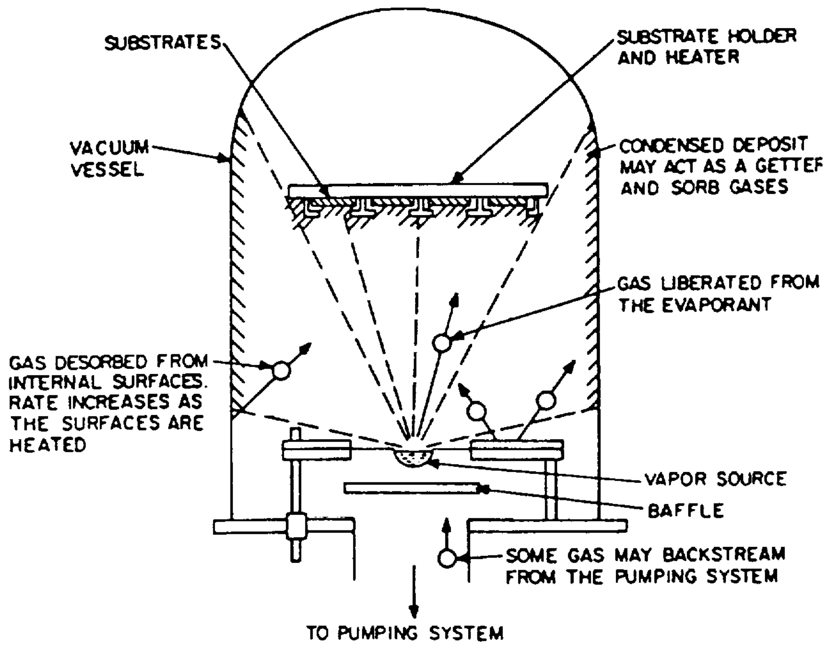

Figure. 3: Schematic of an evaporator.

Large evaporant charges are held in a crucible heated by electron beam or by a resistant heater in the form of a boat or a basket using Joule heating. Although from the point of view of film purity resistance or Joule heating is not as ideal as electron beam heating, but for all practical purposes it turns out to be all right. Since the evaporation process is usually carried out at a sufficiently low pressure (typically in the range of 10^{-6} to 10^{-5} Torr) so that the evaporated atoms undergo an essentially collisionless "line-of-sight" transport. They follow all solid angle relationships and are governed by vapor pressure relationships.

In this connection it is useful to recollect that the mean free path of gas particles is nearly equal to

$\lambda = 5 / p_m \text{cm}$

where p_m is the pressure in milliTorr. Thus at a pressure of 10^{-4} Torr, λ is of the order of 50 cm and about equal to the size of typical vacuum chamber. Another reason to go for low residual pressures is to avoid oxidation of the hot source material and the condensing coating. The rate at which atoms pass into vacuum from a heated source is given by the Hertz-Knudsen equation,

$W = 3.5 \times 10^{22} \alpha p^* (MT)^{-1/2}$ atoms/cm^2-sec

where p* is the vapor pressure in Torr, T is the temperature in °K, and M is the molecular weight in grams. The proportionality parameter α is the evaporation coefficient. It depends on the cleanliness of the substrate and can range from unity for smooth clean surfaces to very low values (10^{-3}) for dirty surfaces [R4], the same can also happen to high vapor pressure materials that evaporate as molecules for which liquid to solid phase change involves a change in degree of freedom. Thus, the vapor pressure, p*, is a very sensitive function of temperature, and is shown in figure 4 for several materials.

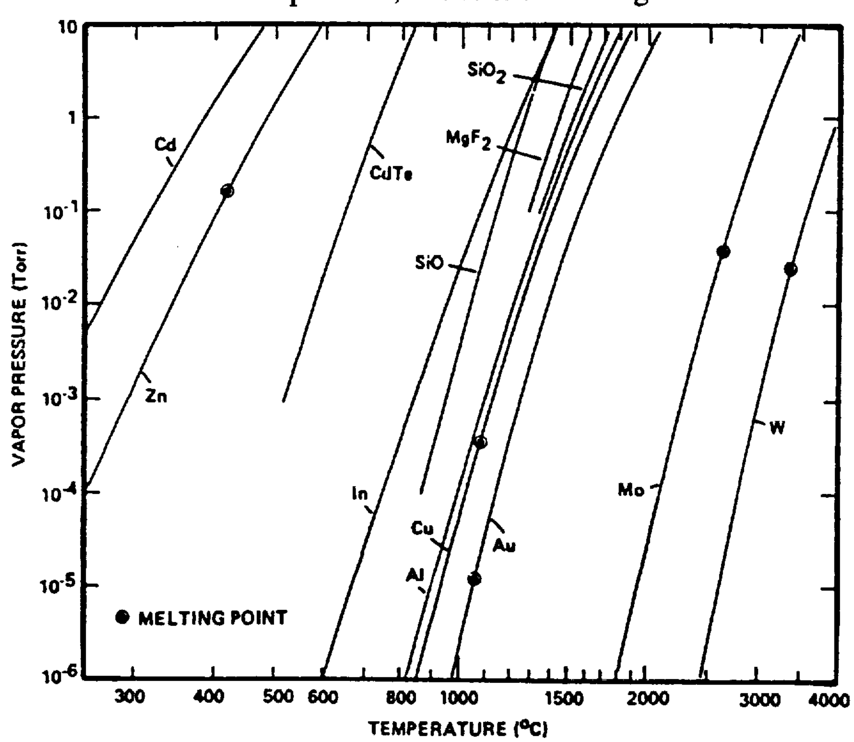

Figure. 4: Equilibrium vapor pressures of various elements.

The table below shows temperatures for evaporating elements commonly used in sensor related processing and from it we see that a source temperature of 1220°C is required for Al to provide $p^* = 10^{-2}$ Torr. We assume that this temperature is used.

TABLE II

Temperatures for commonly used evaporating elements for sensor processing [R3]

Element	Predominant Vapor	Melting Temp(°C) T_M	Temp(°C)at 10^{-2} Torr T	T/T_M
Aluminum	**Al**	659	1220	1.61
Antimony	**Sb_4, Sb_2**	630	530	0.89
Arsenic	**As_4,As_2**	820	300	0.52
Beryllium	**Be**	1283	1230	0.97
Cadmium	**Cd**	321	265	0.91
Chromium	**Cr**	~1990	1400	0.77
Copper	**Cu**	1084	1260	1.13
Gallium	**Ga**	30	1130	4.63
Germanium	**Ge**	940	1400	1.38
Gold	**Au**	1063	1400	1.24
Indium	**In**	156	950	2.85
Lead	**Pb**	328	715	1.64
Molybdenum	**Mo**	2620	2530	0.97
Nickel	**Ni**	1450	1530	1.07
Palladium	**Pd**	1550	1460	0.95
Platinum	**Pt**	1770	2100	1.16
Silicon	**Si**	1410	1350	0.96
Silver	**Ag**	961	1030	1.06
Tantalum	**Ta**	3000	3060	1.02
Tellurim	**Te**	450	375	0.90
Tin	**Sn**	232	1250	3.02
Titanium	**Ti**	1700	1750	1.03
Tungsten	**W**	3380	3230	0.96
Zinc	**Zn**	420	345	0.89
Zirconium	**Zr**	1850	2400	1.26

Two different types of evaporators were used, one was an NRC evaporator model 720, in which the current of nearly 15A was required typically to evaporate Fe, and 10-12A was required to evaporate Al. The second metal evaporator was an e-beam

---

R4 R. Glang, "Handbook of Thin Film Technology", L.I. Maissel and R. Glang ed., McGraw-Hill, New York, p. 1-3 to 1-130.

evaporator called as AIRCO-Temescal Fast Cycle Coater model FC 1800 No. 150, and was mainly used for evaporating Al. High purity evaporating materials, high deposition rates and low residual vacuum was used to assure high purity deposits. Wire and metal foil type sources were provided and a small source emitting from its surface type of geometry was used in resistive evaporations. For the e-beam metal evaporators, extracting voltage was about 10 kV and filament current approximately 150 mA, for a uniform deposition. Sputtering mechanisms were also used for dislodging and ejecting noble metal ions like Au etc. Sputtering apparatus used in the experimental work is now described below.

3.2 SPUTTERING APPARATUS

Most often the source of ions for bombarding the target is from a glow discharge. A simple apparatus using sputtering phenomenon is shown schematically in figure 5. It is a gas filled diode with plane parallel cathode and anode. The cathode is the target and is made of the material to be sputtered. The substrate upon which the film is to be deposited is placed on the anode. This assembly is enclosed in a bell jar that is filled with a rare gas, usually Ar, at a pressure of 10 milliTorr, and a sufficient potential difference is established between the cathode and the anode to cause the gas to breakdown, thereby creating a glow discharge. The sputtering apparatus is usually operated in the so-called abnormal glow region of the glow discharge, because in that region the entire cathode gets involved and the number of ions is large and controllable. Diode sputtering system operates with a dc potential between 1 to 5 KV and a current density of 1 to 10 mA/cm^2 . Electrodes are spaced typically in the range of 1 to 12 cm and their diameters vary between 5 to 50 cm. Deposition rate G is proportional to the ion current I and the sputtering yield S, and is given by the relation,

$$G = C I S$$

where C is the constant of proportionality that characterizes the particular sputtering apparatus. The table below shows sputtering yield for various materials under Ar ion bombardment.

Table III

Sputtering yield of various species under Ar bombardment

Element	Ion Energy (eV)	Sputtering Yield
Au	600	2.80
Bi	500	6.64
Cd	500	7.20
Cr	600	1.3
Dy	500	0.88
Er	500	0.77
Eu	500	5.02
Gd	500	0.83
Hf	500	0.70
In	500	3.25
Ir	500	1.01
Fe	600	1.30
Mn	500	1.9
Nd	500	2.65
Os	600	0.95
Pb	500	4.81
Pd	600	2.40
Pr	500	2.40
Pt	600	1.60
Rb	500	9.20
Re	600	0.40
Rh	600	1.50
Sb	500	2.83
Se	500	3.35
Sn	500	1.20
W	600	5.07

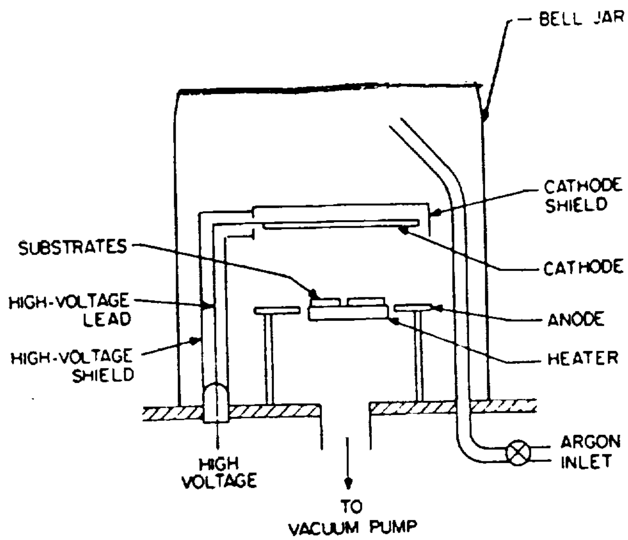

Figure 5. Schematic of a diode sputtering apparatus.

In addition to the mass of the bombarding ion and its energy, the sputtering yield is a function of gas pressure in the sputtering apparatus, because of the fact that many of the ejected ions diffuse back to the cathode when the gas pressure is high. This is important because the power available for sputtering is not unlimited and the only way to increase the ion current without increasing the power is to increase the pressure. The experimental upper limit is about 100 milli Torr with deposition rates of 100 to 500 Å/min, even with materials such as tantalum which have low sputtering yield. A sputtering yield curve for Cu sputtered by Ar is shown in Figure 6. For our usage a Hummer V from Technics Corp. was used and it had a 3'' donut shaped target with magnetic field assistance, giving between 150 - 200 Å /min deposition rate. We have now obtained a Pelco SC5 unit with automatic control, a film thickness monitor and high resolution to get an in house model sputter coater, supplied by the electron microscopy supply center of Ted Pella, Inc. 4595, Mountain Lakes Boulevard, Redding CA 96003. This is a high power unit and capable of producing voltages in excess of 3000V DC at 85 mA. Thus, it would take lesser time in comparison to Hummer V to deposit thick films. In construction, however it is similar to Hummer V, but has a higher pumping speed and power available to be used during sputtering. Right now the vacuum port is designed for a 1/2" I.D vacuum connection but a high speed Edward's pump is attached via a heavy wall vacuum hose and provides vacuum less than 10^{-2} Torr, under usual operating conditions.

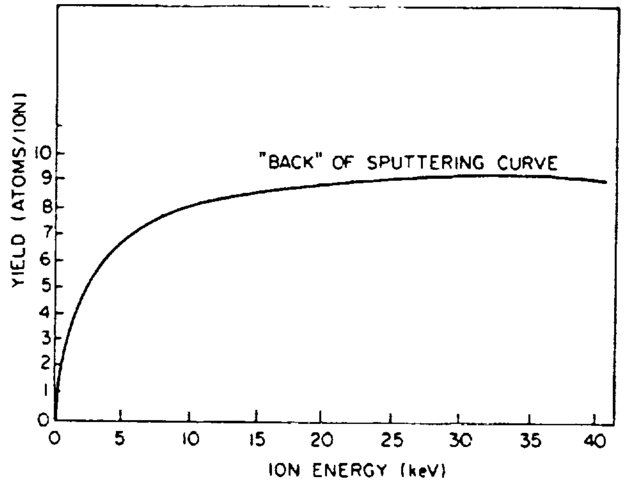

Figure 6: Sputtering yield for copper bombarded by argon ions.

3.3 DEPOSITION UNIFORMITY RESULTS

Experimentally we found that the uniformity of e-beam evaporated Al was pretty good and we could get repeated results as seen in figure 7 (i) below of runs of Al for 4900 - 5000 Å on glass but there was a bit of non uniformity due to pile up at the middle of the electrodes in some samples as seen in figure 7(ii) below.

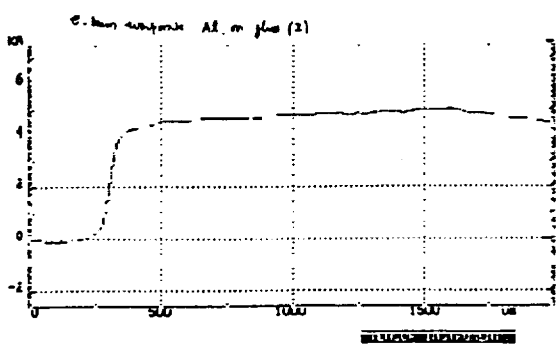

Figure 7(i)

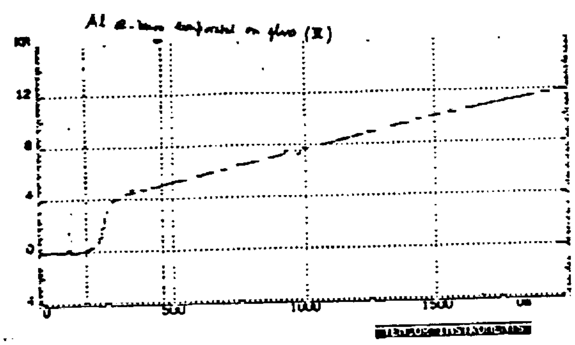

Figure 7(ii)

Sputtered Au-Pd (60/40) film on glass ranged between 450 to 600 Å thick but the surface uniformity was difficult to determine, due may be to globule formation. Silver also showed slightly non-uniform surface but about 400-500 Å thick film was easily obtained. Figure 8 shows the non-uniformity in a typical film. The evaporation method was not very specifically designed for thickness uniformities required and no planetary type rotating target mounts were available, thus, four samples were placed symmetrically, spaced at about 10-11 inches from the basket/boat of the physical vapor deposition system. Further efforts are on the way to get more thickness uniformity from another Joule heated evaporation system.

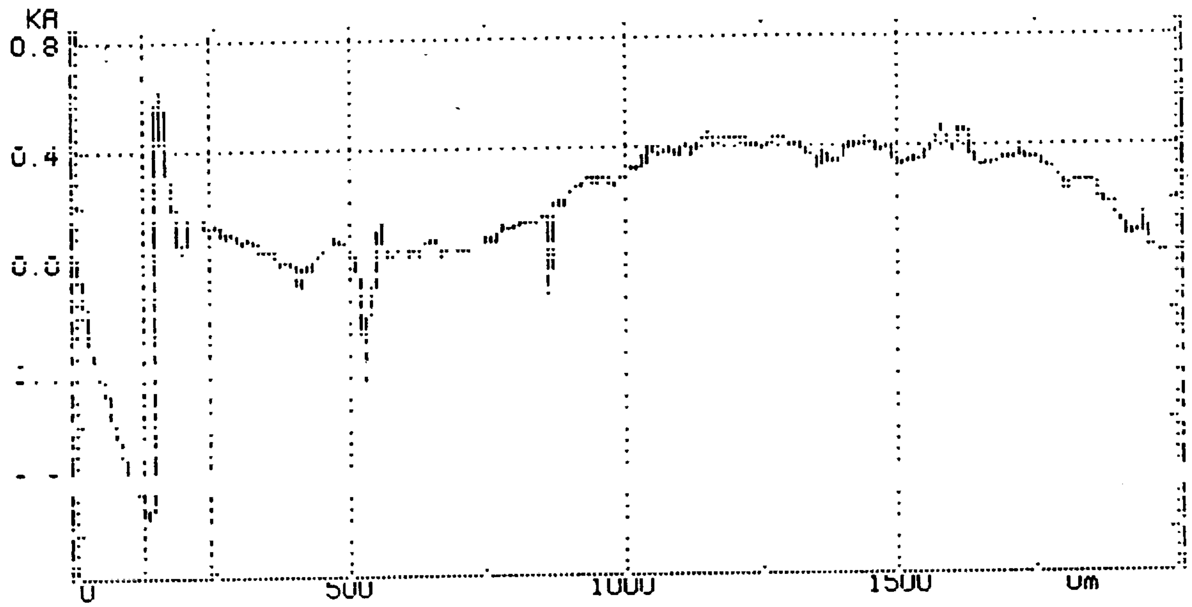

Figure 8: Silver PVD evaporate on glass substrate- stage I

3.4 RESULTS ON FABRICATION ASPECTS OF RESEARCH ON CORROSION SENSORS.

We have developed so far two sets of corrosion sensors on two different substrate materials- regular pyrex glass and sintered alumina. The first stage sensor utilizes only one corroding metal film - aluminum. Gold/palladium (sputter deposited on glass substrates) and gold (on alumina) films as well as silver films are deposited on these using suitably cut masks for each element. The masks have been cut out of a very thin sheet of stainless steel. They were suitably fixed on the substrates using adhesive tape. Aluminum film was mainly evaporated in an electron beam vapor deposition system (AIRCO - Temescal coater model FC 1800 No. 150) , gold and silver was physical vapor deposited in a Denton vacuum evaporator, and the gold/palladium film was sputter deposited. Their thickness were measured later using a Tencor thickness gauge. The latter was also used to check on the uniformity of the thin film deposits along its width. Readings were taken at random in representative locations only. The uniformity was found within ~ 6% over the whole surface.

Stage I Sensor: So far we have prepared two specimens each with the three thin film (TF) electrodes. These have been processed in different systems (on glass in one, and on alumina in the other), and tested for uniformity and thickness and continuity, etc. These electrodes were usually Al, Ag and Au. We are planning to evaluate their electrical resistivity when a suitable test system becomes available. Electrical wiring has also been accomplished using fine gauge copper wire and conductive silver paint-type glue.

Stage II sensor: It has five TF electrodes, has three corrodible working electrodes, aluminum Copper and iron. These are suitably located, one on either side of a centrally located gold counter electrode film and adjoined by silver films at the far extremes, one near each corrodible electrode, such that they can be used as reference for measuring the potentials. Stage II sensors are also made on glass and alumina substrates, two for each kind. Iron electrodes showed high resistivities and did not perform well in corrosion tests. The width of the working electrode in this case(stage II) is reduced to half its value in the stage I in order to facilitate the placement of all five elements on the same substrate. (see Figures 9 and 10).

The thickness profiles of the thin film evaporation deposited representative samples of stage II specimens on alumina substrate are shown in figure 11. These appear to show fairly uniform thickness values with silver showing 810 Å, 1250 Å, iron showing 7300 Å, gold 10,450 Å and aluminum 11,400 Å. More experimental coating work is continuing which will involve electroplating after sputter deposition of TF electrodes to achieve higher aspect ratios and suitable miniaturization. This may also be done by electroless plating if the substrates of commercially available polyimde films are chosen. Non uniformity in alumina substrate has not been of much disadvantage as it does help in increasing the surface area of the film. More work will be done with various NaCl percentage and evaluate the highest demands on aspect ratio of such electrodes. Included in the Appendix are photographs of the Stage I and Stage II microsensors, and research team members and corrosion testing, fog testing and PELCO PC5 sputtering equipment.

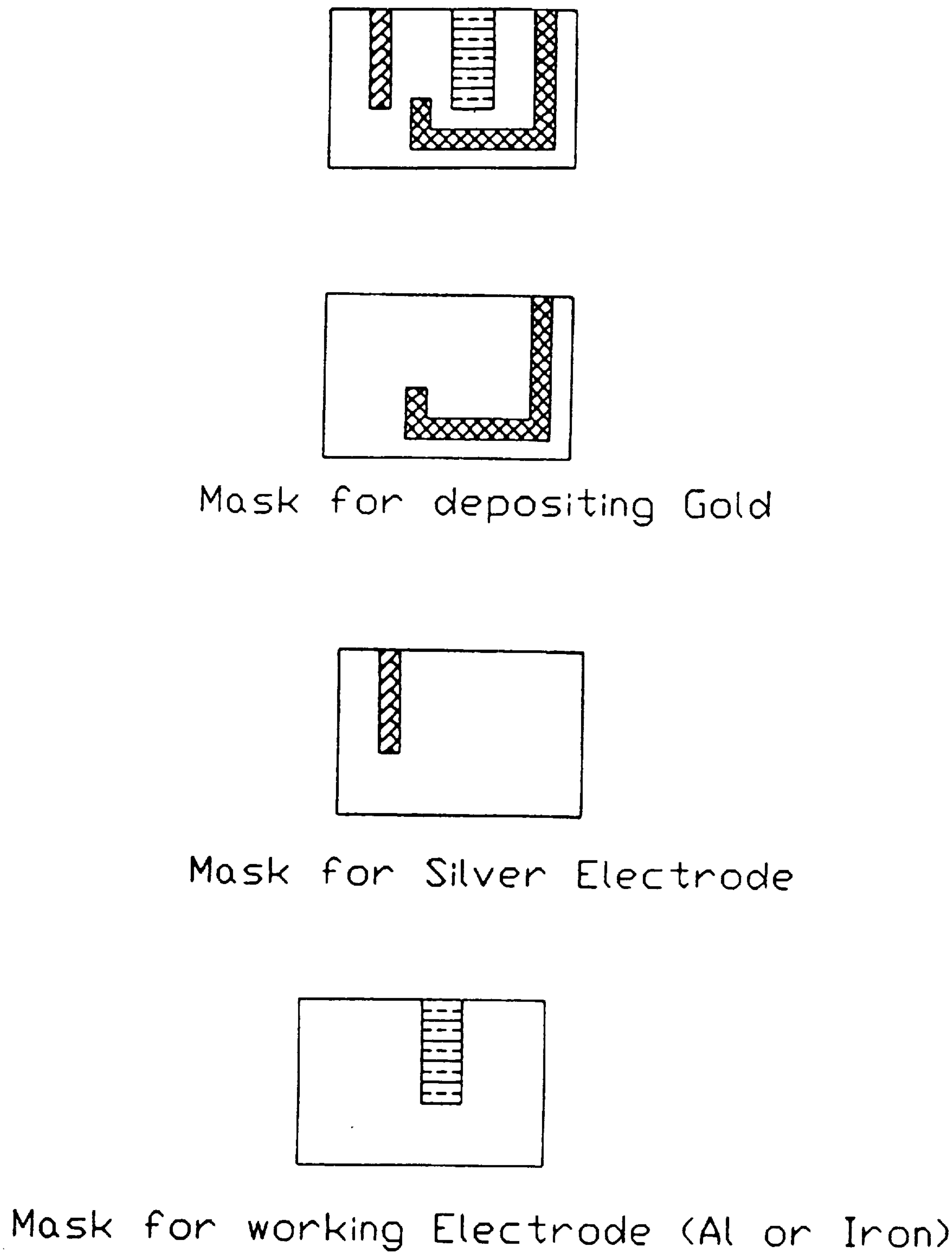

FIGURE 9: Sketch of Microsensor for corrosion monitoring with one working electrode with individual masks as shown - Stage I.

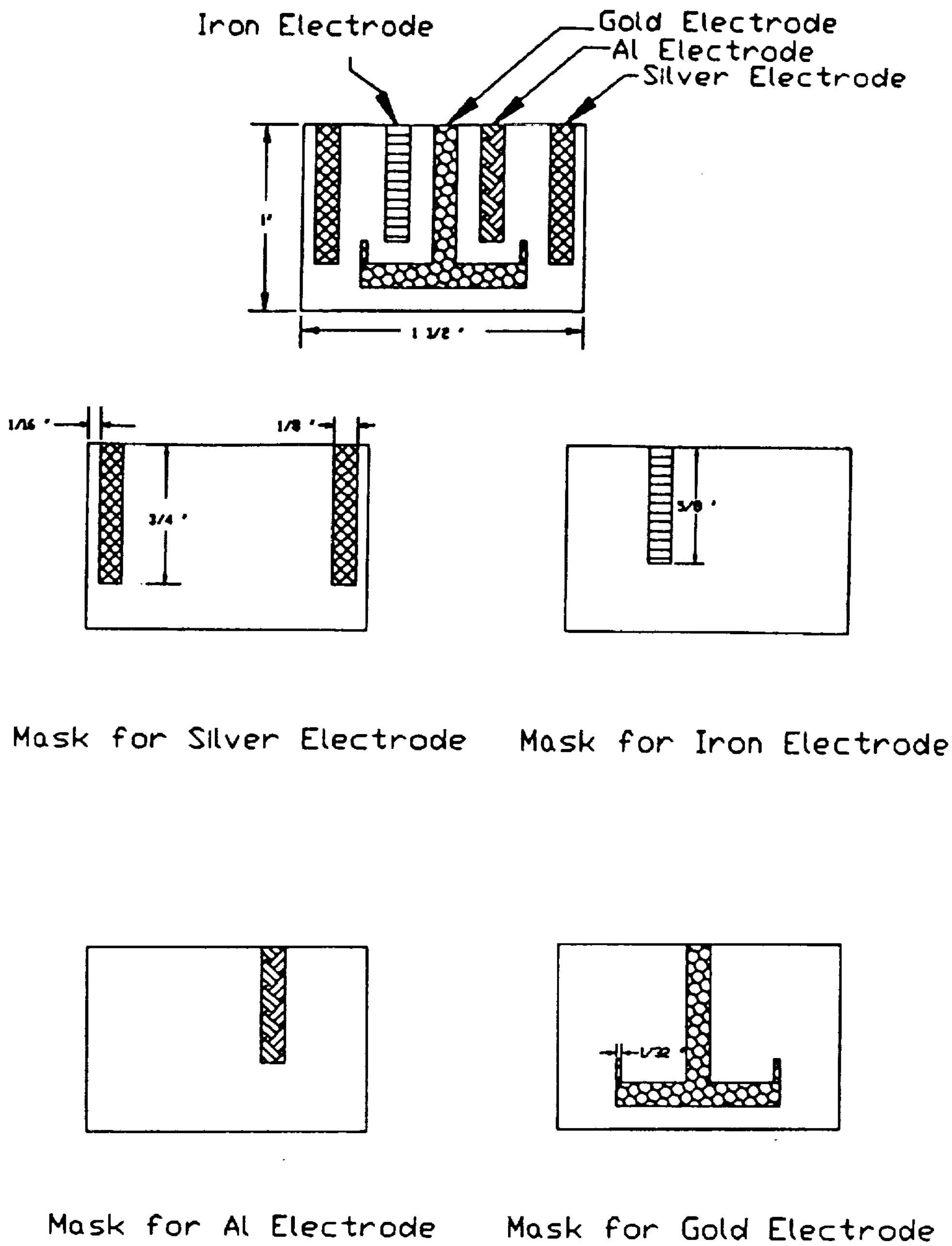

FIGURE 10: Microsensor with two working electrodes - Sketch of microsensor for corrosion for corrosion monitoring - Stage II.

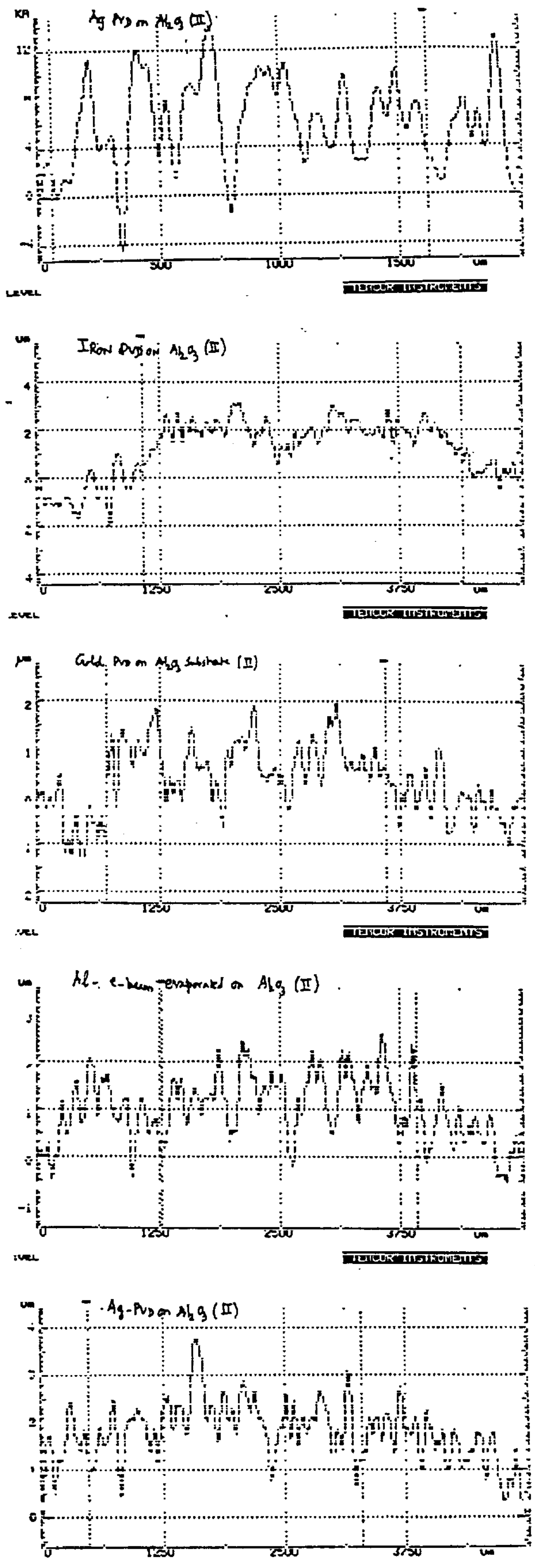

FIGURE 11: Thickness profile Tencor readings of representative sample of stage II microsensor.

ORIGINAL PAGE IS
OF POOR QUALITY

4.0 CORROSION TESTING

Corrosion testing of sensor assemblies is usually accomplished through electrochemical test procedures. The corrosion rate is determined using linear polarization, while total corrosion losses are obtained from increase in resistance of a resistance probe that is allowed to corrode in the same environment. In our program we have used linear polarization technique to obtain corrosion rates of the corrodible metal in the sensor assemblies made.

Two types of sensor assemblies have been made and tested. These are the Stage I three metal thin film assemblies on glass and alumina substrates. Particularly the Al thin film (Al-TF) has been tested in the assemblies Ag-Al-Au on both the glass and alumina substrates. The testing has been both under immersion in various electrolytes as well as in a fog chamber wherein a fog has been created using tap water. In the latter the testing has been under wet-dry cyclic conditions. Within the limited time available for testing, exterior exposures and evaluations of real atmospheric corrosion could not be carried out so far.

Besides the three metal assemblies, the Stage II five film assemblies with two corrodible working metals have also been tested. Of these, testing has been accomplished on the Ag-Al-Au-Cu-Ag assembly on Al and Cu thin films individually in the three member assembly mode, such as Ag-Al-Au and Au-Cu-Ag, as well as in the Al-Cu coupled mode, i.e. in the Ag-Al/Cu-Au mode. As on the three electrode assemblies, the testing has been under immersion in various electrolytes as well as in the fog chamber under a fog created with tap water. In the latter, the five-electrode assembly has been tested under wet-dry cyclic conditions.

During the actual exterior exposure, corrosion occurs by the condensation of moisture from the atmosphere at high humidity levels and this condition is approximated by the wetting half of the fog test cycle. In the exterior, not only the condensation does not occur at low enough humidities (say at <50% RH) and elevated temperatures (say above 20-25 deg.C), as prevalent during the day time , the already condensed moisture evaporates, leading to drying. The drying may be complete on bold, sun-hit surfaces if the temperature is high enough, but the surface may not dry totally in sheltered locations. Corrosion would be continuous in such places where the electrolyte film or wet condition is always maintained.

Some places on structures continuously maintain pools of water and in these cases corrosion would resemble continuous immersion conditions. Exactly how much evaporation of already condensed moisture film occurs at various locations is not well defined. Such data is needed to gauge the extent of corrosion.

Corrosion rates under various kinds of exposures are needed in order to judge the extent of corrosion. Corrosion builds up corrosion product films or layers which would continuously alter the corrosion rates. The nature of the corrosion product formed, its porosity and electrolyte or ion permittivity, its stability and transformation characteristics, etc. all have a bearing on the continuous corrosion process and its rate. Macropassivation is possible in some instances where the corrosion product layer forms a compact adherent protective mass on the surface. Such is the case when amorphous corrosion products form on alloy steel surfaces. On the contrary iron sulfide formed on steels is porous; likewise the corrosion products formed on copper in chloride environments are porous. However, the regular passive film on stainless steels is dense and protective of the metal. In such cases, the degradation of the passive film by depassivation processes would be of interest. On aluminum, however, the film that forms could assume different characteristics. The nature of the films formed on aluminum alloys under chloride-containing marine type atmospheres would be of interest in atmospheric corrosion studies.

The wetting and drying characteristics of various metal surfaces, especially under prevalent conditions of debris accumulation and/or corrosion product formation, are not well defined. Some of the corrosion products are hygroscopic and do not dry at all, especially in sheltered locations. The drying is at best on the surface of the corrosion product layer, whereas the interior of the layers at the metal-corrosion product interface would stay wet. The corrosion would continue.

The drying time introduces re-formations of some of the crystalline corrosion products that are porous. For example, on iron and steels α-FeOOH crystals start forming through the amorphous rust dissolution and recrystallization from the solution. The formed crystals are uniquely whiskered or are of the sheet type with lots of pores in between them. Such structures are not protective of steel.

However, the pores formed in the corrosion product layer can be plugged by precipitates of other kinds, say from selected precipitation-type inhibitors. For example, it is well known that phosphates and benzoates precipitate and plug the harmful pores. The chemical conversion-type compounds should all be helpful. So if a chemical conversion coating is applied, it should provide some benefits.

In prior sensor evaluations, these aspects of the problem have not been considered. Any corrosion evaluations in the exterior involving corrodible sensor elements should be able to explain the above raised points. Previous studies with the sensors have been to determine the corrosivity of the atmospheres qualitatively. Quantitative evaluation of the corrosivity of the atmosphere would obviously require an understanding and precise determination of the extent of corrosion under corrosion product films. No attempts have been made in the past to determine the corrosion rate of the actual metal in the member experiencing atmospheric corrosion.

The following points need to be clarified in the corrosion testing with the sensors:

1. How thin the condensate moisture film can be in order to carry current and cause meaningful corrosion?
2. How is the corrosion rate affected by the thickness of the condensate film on the sensor complex?

3. How does condensation and evaporation occur in the exterior and how these would affect the corrosion rate?
4. What are the effects of corrosion product formation on the water retention and corrosion rate?
5. What are the effects of phase transformations in the corrosion products?
6. How can the results from different sensors be made to unify and yield the same corrosion data?
7. How can the results from resistance probes be made truly reflective of the actual total cumulative corrosion damage of a given metal in a structural member?

These are some of the questions that are being raised today. In addition the available sensors do not fulfill all the functions. For example, they do not define the actual corrosion potential of a metal in exterior exposure, nor its actual corrosion rate.

With the above in mind, we have chosen to study the corrosion characteristics of actual structural metals in sensor assemblies. To be able to measure the true corrosion potential, one should be able to include a reference electrode in the sensor complex itself. Though we have not accomplished this feat yet, it is one of our goals to evolve a thin film reference electrode to read the corrosion potential of the corroding member. Our goal includes also the determination of the actual corrosion rate as well as the actual cumulative corrosion loss at any location in an actual structural member experiencing atmospheric corrosion. Our corrosion testing to date addresses some of the issues raised above.

4.1 CORROSION TESTS PERFORMED

In the testing of atmospheric corrosion sensors, actual exterior exposure is very vital. However, prior to actual exterior utilization, the exterior exposure conditions can be simulated in the laboratory in accelerated tests and the sensor behavior tested. One such test is the exposure to cyclic fog in a fog chamber. We have carried out the cyclic fog testing in one hour full cycles, with 30 minutes for the wetting fog accumulation part and the other 30 minutes for the drying part, accomplished by blowing warm air with a hot air blower through a port. The fog is created continuously during the 30 minute wetting part of the cycle by atomizing the selected solution with compressed air at 15 psig pressure. In our program to date we have used only tap water as the source for the fog and performed the tests at room temperature in the fog chamber, that is not utilizing any heating of the environment in the chamber.

In the limited time available, we could handle only the Al and Cu thin films. Initially we immersion tested the Al thin film in the Stage I sensor samples made by using the three electrode configuration, Al-TF for the working electrode, Au-TF for the counter electrode, and an external calomel electrode; the Ag-TF was used sparingly, only to get a bearing on the corrosion potential with it and its shift from the actual value, measured with the standard calomel electrode.

The testing was started by studying the basic linear polarization of bulk metal samples under immersion. Four electrolytes were generally used in immersion testing. These were: distilled water, tap water, 0.1% NaCl solution in distilled water, and 3.5% NaCl solution in distilled water. The specimens were kept immersed in the solution for at least 30 minutes prior to the start of the tests. Linear polarization testing was carried out thereafter. First the corrosion potential was determined by manually adjusting the potential setting (E)on the potentiostat such that the current (I) moved to zero. Then the base potential was fixed at 30 mV below this value and anodic polarization scan was made with a scan rate of either 1mV/sec or 0.5mV/sec. Both gave nearly similar results and good scans. The scans were made two separate times. The first time the current was measured and plotted on a linear scale, i.e. it gave rise to the E vs. I plot. The second time the current measured was plotted on a log scale which resulted in the E vs. log I plot. From the former, the corrosion potential E_{corr} and the polarization resistance Rp (=dE/dI) could be obtained. The latter is multiplied usually by the area of the electrode involved so that it will be given in Ωcm^2 units. The polarization resistance with this unit is denoted as

Rp*. The E vs. log I plot gives rise to the two Tafel slopes, βa and βc, as well as the corrosion potential and the Tafel lines-extrapolated corrosion current. Dividing the current with the area of the electrode, the I_{corr} in μAcm^{-2} units is obtained. From the two Tafel slopes βa and βc and the polarization resistance Rp*, the corrosion current density is again obtained by using the Stern-Geary equation:

$$I_{corr} = [\ \beta a.\ \beta c\ /\ 2.303(\ \beta a + \beta c)]/\ Rp^* =\ B/Rp^*$$

The Tafel slopes are given in mV per decade change in current on the linear part of the respective curves. E_{corr} is given in mV(SCE) when standard calomel electrode is used. In other cases it is given in mV against the standard used. Since we have not made the Ag-TF into reference electrode yet, when we used it in the tests, it gave a pseudo-potential of the working electrode, using which its variation as a function of exposure and corrosion could be defined.

A junction box with five terminal inputs and three terminal outputs was made in our electronic shop to which the three electrode or the five electrode sensor complex thin film electrodes could be connected. The outgoing leads from the box were connected to the three terminals of the potentiostat - that is to the working, counter and reference electrode terminals. The five inputs to the box were in the sequence Ref.1(Ag-TF)-W1(Al-TF)-Counter(Au-TF)-W2(Cu-TF)-Ref.2(Ag-TF). When the three electrode specimens were under test, only the first three input terminals were used. Suitable switches enabled operation of either set alone, in which case the corrosion characteristics of the Al-TF or Cu-TF were individually tested, although they were on the five electrode sensor complex. The two working electrodes could be shunted together and studied against Au-TF as counter electrode. This is the way we have carried out the experiments so far. However, they could be connected to the potentiostat so that one of them is used as the counter electrode and the other the working electrode, although in our design of the five electrode sensor complex the Au-TF is in the middle of the two and has to be ignored. This has not been attempted so far.

In immersion testing the specimens were rinsed with distilled water after the tests, dried with a blower with warm air and stored in a desiccator. They were tested a few days later in similar configuration in similar solution to determine the sensor's aging characteristics due to corrosion.

Testing in the fog chamber was carried out in cyclic mode as already explained. A small hole was drilled through the chamber wall and the wiring leads could be taken out of this hole for connection to the junction box. The potentiostat was stationed near the fog chamber while carrying out these tests. One hour total cycle time was found to be optimum, of which 30 minute was in the fog wetting part and the remaining 30 minutes in the drying part. In the future when automatic data accumulation with the computer or with a data logger would be feasible, the cycle time would be attempted to be reduced to 1/2 hour each, with 15 minute for fogging and 15 minute for drying. Such cycles have been utilized in all of our previous studies, and the corrosion data obtained on steel samples have been found to yield approximately similar data as in exterior exposures. This means that each 1/2 hour cycle data corresponds to 1 day actual exposure to nearly 100% humidity conditions as prevalent in Louisiana and in coastal areas. The specimens were cleaned, dried and stored in the desiccator after each test.

4.2 TIME OF WETNESS AND VARIATION IN WETNESS

Wet-dry cyclic fog testing wets the specimen over a given period of time and the moisture film condenses on the sensor surface and builds up in thickness and form. The current would increase gradually and the current increase is reflective of the moisture film formation and growth kinetics. Likewise, during the drying period the film evaporates steadily and leaves the surface. How much evaporation occurs and the kinetics of evaporation can be studied by following the current decay. These are accomplished by using the sensor as a current monitor. Fixing the working electrode at a specific potential, say at a cathodic potential such that it won't undergo corrosion while the current flows, the current build-up during the wetting, fogging period and its decay during the drying part of the cycle can be followed. This has been done in our fog testing program with the Al-TF electrode in the three electrode sensor, as well as by using a spent (i.e. working electrode corroded off) -sensor complex, but using only the Ag-Au-Ag in the five electrode complex for the purpose of tracking the current. A typical current build-up and decay record is given in Figure 12. As can be seen from the figure, the current rises nearly exponentially upto a certain intermediate level, then jumps up sharply to the peak value and stays at this value till the drying part of the cycle starts. At the start of drying the current drops sharply to the intermediate value and then decays exponentially to the base value. Oscillations that occur at the end of the drying cycle indicate extreme instability of the wet film and its step-wise removal from the surface. More work needs to be carried out further on this aspect of electrolyte film formation and its evaporation.

Only two electrolytes are planned to be used in the fog chamber - the tap water and the 0.1% NaCl solution in tap water. Experiments with the former have been conducted in this fiscal year. Future experiments will utilize also the latter electrolyte.

4.3 FOG TESTS

Fog tests have been conducted on the Ag-Al-Au Stage I sensor complex as well as on the Stage II Ag-Al-Au-Cu-Ag complex. In the latter the testing has yielded individual corrosion data for the Al and Cu TFs as well as the data for the Al/Cu couple against the Au counter electrode. The individual corrosion potentials as well as the potential of the couple against Au were determined in selected cycles. The polarization was carried out as explained before using the Ag-TF as the reference electrode. Thus a pseudo-corrosion-potential is determined in the fog chamber. After the Ag-TF is converted to a suitable reference electrode, the actual corrosion potentials against Ag reference electrode would be determined. In all cases polarization runs were started in the wetting part of the cycle after considerable initial time having been allowed for stabilization of the electrolyte film. In the 30 minute fogging period this was after about 15 minutes after the start of fogging.

Figure 12 shows the current steadying after about 15 minutes during wetting by fogging. The tests were conducted and finished prior to the start of the drying half cycle.

As stated already, tests were carried out in 1 hour cycles of fogging and drying, each occupying 30 minute portion of each cycle. A controller was set suitably to accomplish this. During the fogging part of the cycle the controller automatically opened a solenoid valve and allowed compressed air at 15 psig to flow through the port for atomizing purposes. During the drying part of the cycle the solenoid valve shut closed and the drying blower came up. Warm air was blown during the drying half of the cycle. The wetting and drying repeat themselves for a preset number of cycles. In our current test program, we have tested only upto 50 cycles over a two day period and polarization data have been collected manually in approximately five cycle intervals. The variations of the electrochemical corrosion parameters such as corrosion potential, corrosion current and the polarization resistance as a function of exposure could be obtained.

4.4 RESULTS AND DISCUSSION

Results of immersion tests with thick specimens of an Al-alloy, and two different steels ASTM A 36 and A 588, and electronic copper are given in Table IV. The data are used to orient the tests. In the future, bulk specimens are planned to be tested in the atmospheric corrosion test program with the sensors and the preliminary results obtained here would be helpful.

Immersion test results for the Al-TF in the Ag-Al-Au sensor assemblies on glass and alumina substrates are given in Table V. In 3.5% NaCl solution, the corrosion potential shifted to a more negative value when tested for the third time after 8 days and the polarization resistance was also found to be low. The corrosion current had increased drastically. These results point to the inability of the Al-TF to retain its passive film on the surface and corrosion in the sea water equivalent 3.5% NaCl solution would be severe. Huge pits were noticed on the specimen surface and the whole micron-thick film corroded

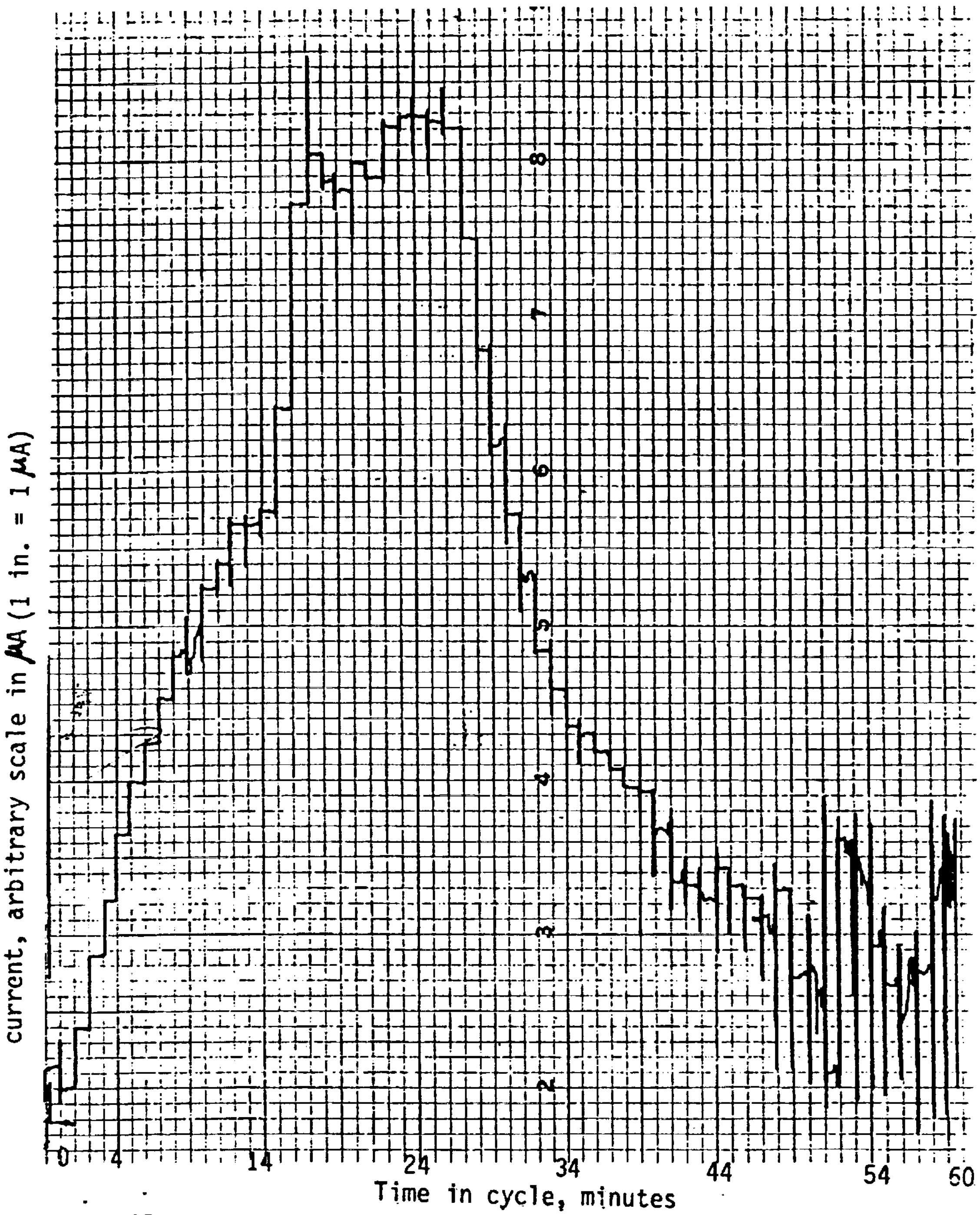

Figure 12 Current variations at a set potential as a function of wetting by fog and drying. (wetting during the first 27 minutes)

Table IV
Electrochemical data from immersion test on thick metals

No.	Metal	Electrolyte	Ecorr(mV) (SCE)	Rp* (Ω .cm ^{2})	Icorr (μ A/cm ^{2}) Interpold.	Calcd.
1	Al-plate	3.5% NaCl	-731	7020	0.44	0.56
2	A-36 steel plate	3.5% NaCl	-652	752	2.90	4.27
3	A-588 steel	3.5% NaCl	-688	1439	4.16	5.37
		0.05% NaCl	-650	4073	1.15	1.39
		tap water	-657	6464	0.73	0.96
4	Electronic copper	3.5% NaCl	-222	5250	1.13	1.01
		0.1% NaCl	-63	104500	0.271	0.033

off soon. High corrosion rates also are indicated in 0.1% NaCl solution. The latter resembles approximately the electrolyte condensates in the coastal areas, that is in marine atmospheres. On the contrary the corrosion potential is higher in tap water, about 400 mV higher, and the corrosion rate is smaller, nearly by an order of magnitude. The potential is still higher, about 100 mV more, in distilled water than in tap water and the corrosion current is smaller by yet another order of magnitude. Figure 13 indicates the linear and log polarization plots of the Al-TF electrode in distilled water. These results are all explicable from the conductivity of the electrolytes and the passivation and depassivation characteristics of Al-TF in the tested electrolytes. Chloride-containing solutions would lead to depassive attack on the Al film and initiate pitting. These are verified.

Table VI summarizes the results from the Al-TF in the Ag-Al-Au Stage I sensor on alumina substrate in the fog test with tap water fog. Typical linear and log polarization plots from the 15th cycle are given in Figure 14. During these tests the specimen surface stayed wet considerably longer and drying was much less effective as ambient air was being used for drying. Data in Table VI shows that the corrosion potential increased slowly at the beginning , from about -535 mV to about -500 mV, for about 30 cycles, then suddenly increased in the 31st cycle to about -375 mV and increased once again to -37 mV by the 50th cycle. The polarization resistance seems to rise moderately till about the 31st cycle and increase sharply when the potential increased. The corrosion current seems to decrease steadily by a factor of four.

The rise in corrosion potential, the increase in the polarization resistance and the accompanying drop in corrosion current are all indicative of the Al-TF attaining more and more passivation. The sudden jump of corrosion potential on the 31st cycle is indicative of such an onset of passivation. There is a small drop in corrosion current associated with this phenomenon.

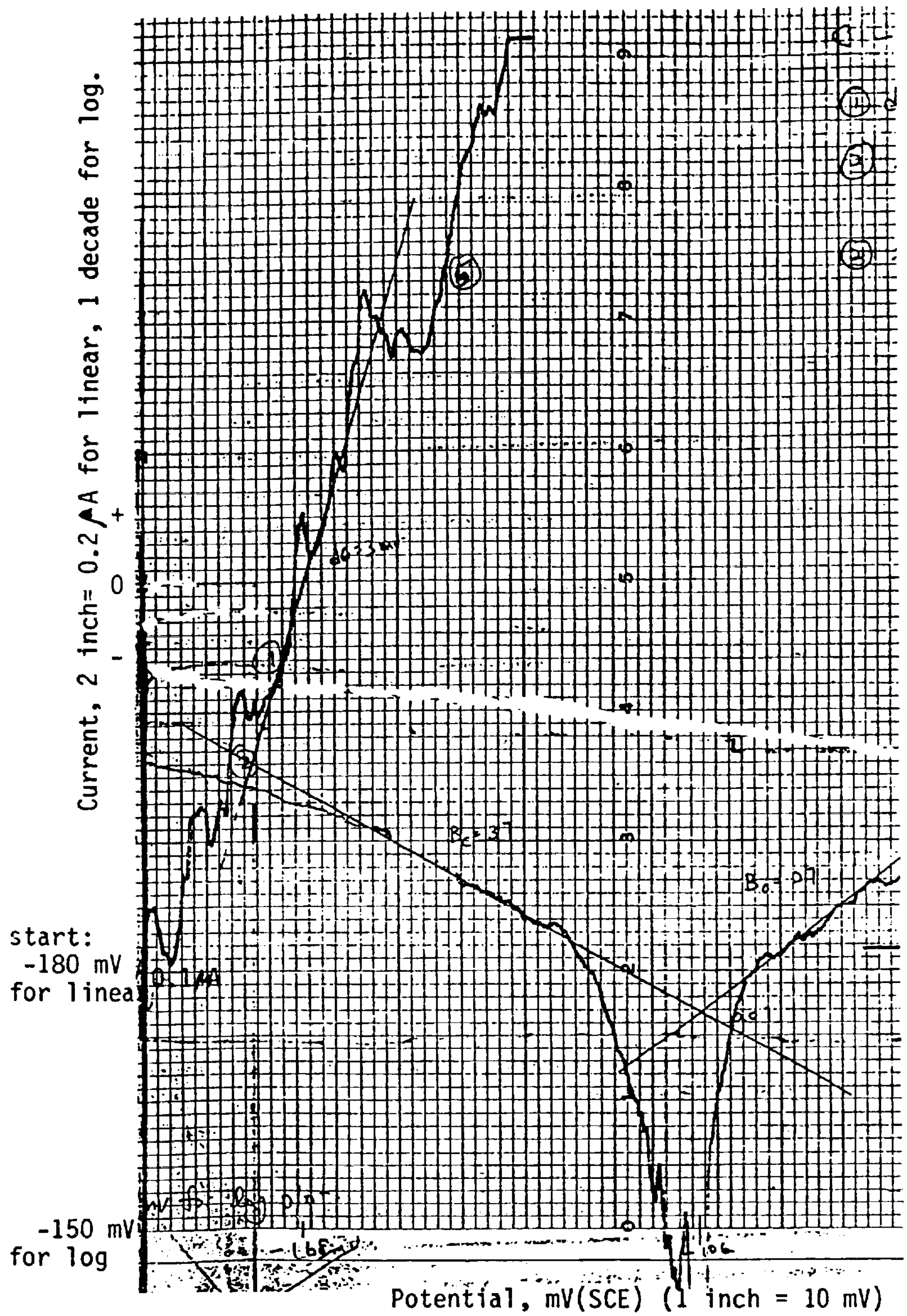

Figure 13 : Linear and log polarization diagrams of Al-TF in distilled water.
Linear: starting potl.= -180 mV; scan rate =0.5 mV/s
X-axis: 1 inch = 10 mV; Y-axis: 1 inch = 0.1 μA.
Log.: starting potl. = -150 mV; scan rate = 0.5 mV/s
X-axis: 1 inch = 10 mV; Y-axis: 0.1 μA at 2 inch, also 2 inch = 1 decade I rise.

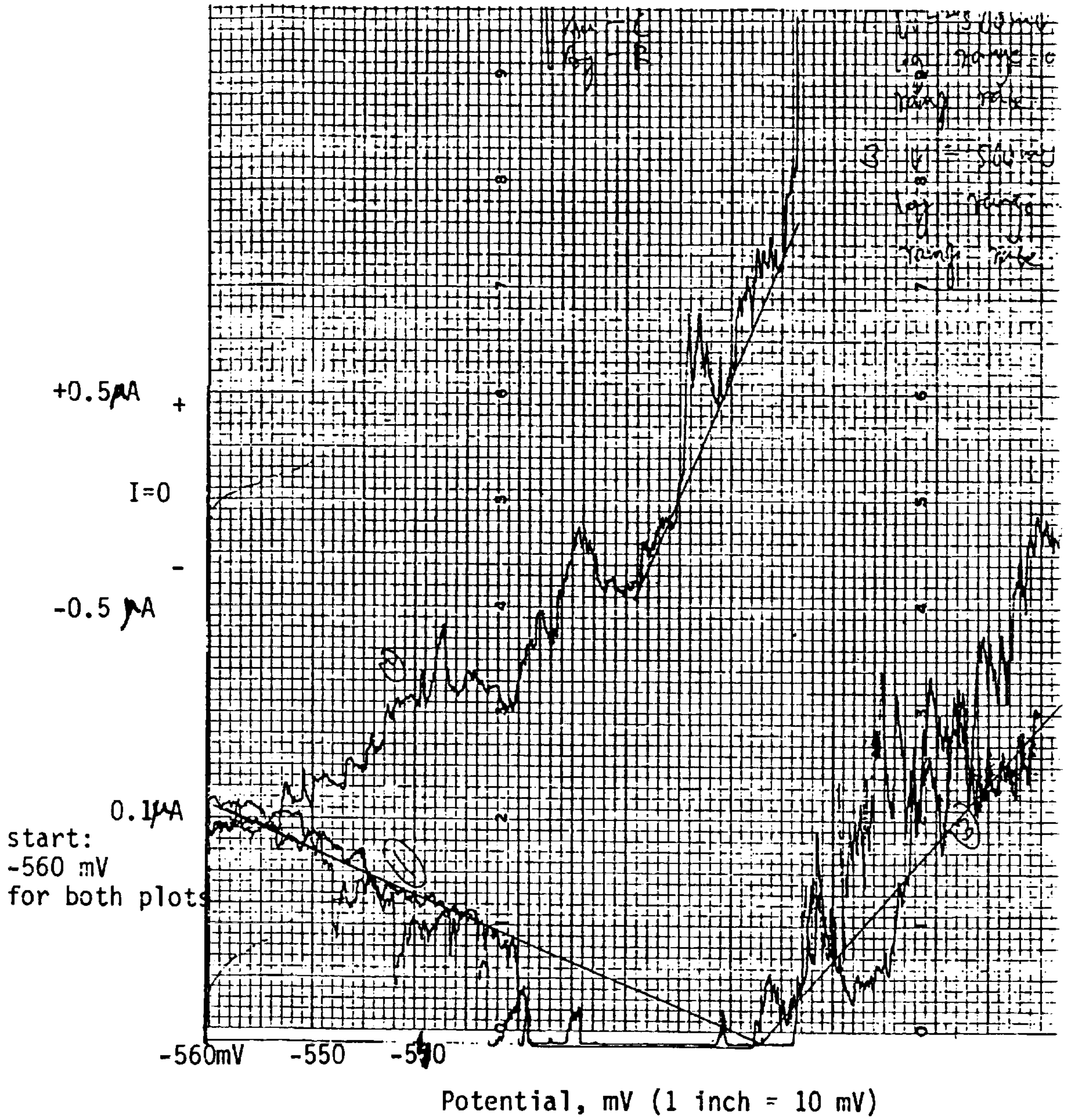

Figure 14: Linear and log polarization diagrams for Al-TF in fog test with tap water.
cycle # 15, wetting part
linear: starting potl. = -560 mV (Ag-TF ref.)
X-axis: 1 inch = 10 mV; Y-axis: 1 inch = 0.5 µA.
log.: starting potl. = -560 mV (Ag-TF ref.)
X-axis: 1 inch = 10 mV; Y-axis: 0.1µA at 2 inch
also 2 inch = 1 decade I rise.

Table V:
Electrochemical data from immersion test of Al thin film in Stage I Ag-Al-Au sensor

Test period	Substrate	Electrolyte	Ecorr(mV) (SCE)	Rp* ($\Omega.cm^2$)	Icorr (μ A/cm ^{2}) Interpold.	Calcd.
first	glass	3.5% NaCl	-626	8580	0.63	0.59
after 1 day	glass	3.5% NaCl	-618	4080	0.51	0.52
after 8 days	glass	3.5% NaCl	-742	96	4.14	12
first	alumina	3.5% NaCl	-633	224	6	19.5
first	alumina	0.1% NaCl	-611	270	10.4	12.4
first	alumina	tap water	-227	1750	1.28	3.53
after 2 days	alumina	tap water	-427	1540	1.55	2.75
first	alumina	distilled water	-125	216000	0.12	0.02

Table VI:
Electrochemical parameters for Al thin film corrosion in Fog test with tap water fog

Cycle Number	E_{corr} (mV) (against Ag-TF)	R_p* (Ω .cm ^{2}) (x 10^4)	I_{corr} (μA/cm^2) (interpolated)	I_{corr} (μA/cm^2) (calculated)
3	-535	2	--	--
4 (wet)	-267	0.15	--	--
4 (dry)	-534	0.14	0.04	3.46
15	-501	0.16	0.04	3.49
20	-508	0.36	0.02	1.2
25	-514	0.29	0.03	1.35
31	-502 & -373	0.43	0.01	1.3
41	-375	1.53	0.02	0.98
46	-370	1.48	0.02	0.84
50	-37	1.53	0.016	0.92

Table VII gives the results from immersion testing of the Ag-Al-Au-Cu-Ag sensor assembly. It can be noted that generally the Cu-TF shows more corrosion current than the Al-TF in the complex under similar test conditions. This is obvious from the results of these electrodes tested with distilled water and 3.5% NaCl solution. The results can be interpreted as due to passivation of Al-TF, whereas the Cu-TF does not get passivated. Data for the Al-TF in the tap water indicates that the corrosion potential increases as the film corrodes, the polarization resistance should correspondingly increase (results of the third test after 10 days seem to confirm this), and the corrosion current drops. Ignoring the results of test after 14 days, the potential of the Cu-TF remains nearly the same, its polarization resistance seems to double and the calculated corrosion current density seems to decrease. However the currents can be assumed to remain nearly the same from the results of the second and third tests on the 7th and the 10th days.

In the 0.1% NaCl solution, corrosion potential of the Al-TF is found to rise, with an accompanying increase of polarization resistance and reduction in the corrosion current density. These are indicative of the passivation taking place on the film. Apparently, the film tested in the latter solution also acquires passivation, so long as it is not kept immersed in the solution for long periods of time. The data from Cu-TF in tests with this solution seems to show slight variations indicating probably the lack of passivation in the Cu-TF in the 0.1% NaCl solution. Uniform corrosion can be inferred for the Cu-TF in this electrolyte as well as in tap water.

Considering the behavior of the Al/Cu TF couple tested against the Au-TF counter electrode, it can be observed that the corrosion potential obtained is generally in between the values of the two individual metal films. Also the value is closer to the higher potential of the two. Only in two cases are the values of the potential of the couple outside of the range between the two individual potentials and locate slightly below the lower potential value. For example, in the case of the test with the 0.1% NaCl solution the third test conducted on the 16th day showed a potential of -62 mV for Al-TF, -115 mV for the Cu-TF, but a value of -125 mV for the mixed electrode Al/Cu. Similar result is also for the

Table VII: Electrochemical corrosion paramaters of Al and Cu thin films individually and in coupled modes in immersion tests in various electrolytes.

Specimen		Aluminum TF				Copper TF				Al-Cu TFs coupled			
Electrolyte	Test period	E_{corr} (mV,SCE)	R_p* ($.cm^2$) ($x10^5$)	I_{corr}($A.cm^{-2}$) extrd.	calcd.	E_{corr} (mV,SCE)	R_p* ($.cm^2$) ($x10^4$)	I_{corr}($A.cm^{-2}$) extrd.	calcd.	E_{corr} (mV,SCE)	R_p* ($.cm^2$) ($x10^4$)	I_{corr}($A.cm^{-2}$) extrd.	calcd.
DW	first	-65	1.15	0.06	0.08	-20	5.04	0.27	0.34	-26	7.56	0.19	0.28
TW	first	-151	1.37	0.056	0.102	-43	3.24	0.016	0.527	-87	2.81	-.097	0.278
	after 7 days	-13	0.79	0.11	0.146	-42	8.8	0.22	0.163	-28	6.12	0.19	0.25
	10 days	-108	5.8	0.007	0.016	-41	6.84	0.14	0.24	-39	13.7	0.057	0.092
	14 days	-34	0.105	0.009	0.003	-19	3.3	0.33	0.502	-23	7.5	0.133	0.170
0.1% NaCl	first	-121	2.84	0.05	0.086	-143	1.8	0.33	0.404	-134	2.9	0.15	0.186
	after 9 days	-63	4.75	0.013	0.023	-170	3.69	0.103	0.183	-144	5.62	0.139	0.166
	16 days	-62	9.6	0.013	0.021	-115	1.22	0.38	0.509	-125	1.97	0.15	0.226
3.5% NaCl	first	-178	3.1	0.058	0.062	-254	0.324	1.72	2.77	-256	0.864	0.86	1.043

Electrolytes: DW = Distilled water; TW = tap water; 0.1% NaCl = 0.1% NaCl solution in distilled water; 3.5% NaCl = 3.5% NaCl solution in distilled water.

3.5% NaCl solution, but here only one data point was recorded. The non-passivating Cu-TF seems to control the corrosion characteristics of the couple in the tap water and 0.1% NaCl solution, for in these all the corrosion parameters are found to remain nearly steady. It can be noted that the current densities given for the couple have been derived by dividing the actual corrosion currents by the total area of the two thin films in the couple, that is by the total area obtained by adding the areas of the Al and Cu TFs in the coupled mode. If, however, only the area of the Cu-TF is used, since it corrodes with a higher current density than the Al-TF, the value would be nearly doubled and come closer to the values of Cu-TF. Thus it appears that in the Al/Cu couple it is the Cu-TF that corrodes. This needs to be verified by testing the two in galvanic couple mode further, that is by taking Al-TF as the counter electrode and the Cu-TF as the working electrode.

Figure 15 carries the polarization plots of some of the Al-TF, Cu-TF and the Al/Cu combined couple against the Au-TF counter electrode in the first test in tap water conducted. These plots are given for illustration purpose only.

Finally, Table VIII contains the results obtained with the 5-electrode sensor in the fog test. In these tests, the conditions of wet-dry cycling were slightly altered such that better drying was obtained this time as compared to the previous test with the Al-TF in the 3-electrode assembly. The corrosion potential of the Al-TF seems to increase only slightly, from about -143 mV to about -86 mV. (The potential is the pseudo-potential measured against the Ag-TF on the sensor assembly). The polarization resistance seems to decrease with a slight increase in corrosion current. Results appear to be varying and the above conclusions need to be treated as tentative.

On the contrary, the potential of the Cu-TF seems to remain nearly steady. There seems to be a decrease in the polarization resistance, but the corrosion current seems to oscillate around a mean value. The calculated value of the corrosion current density is high as in the case of immersion. Considering the unsteady behavior, it can be inferred that the Cu-TF is undergoing uniform corrosion without passivation.

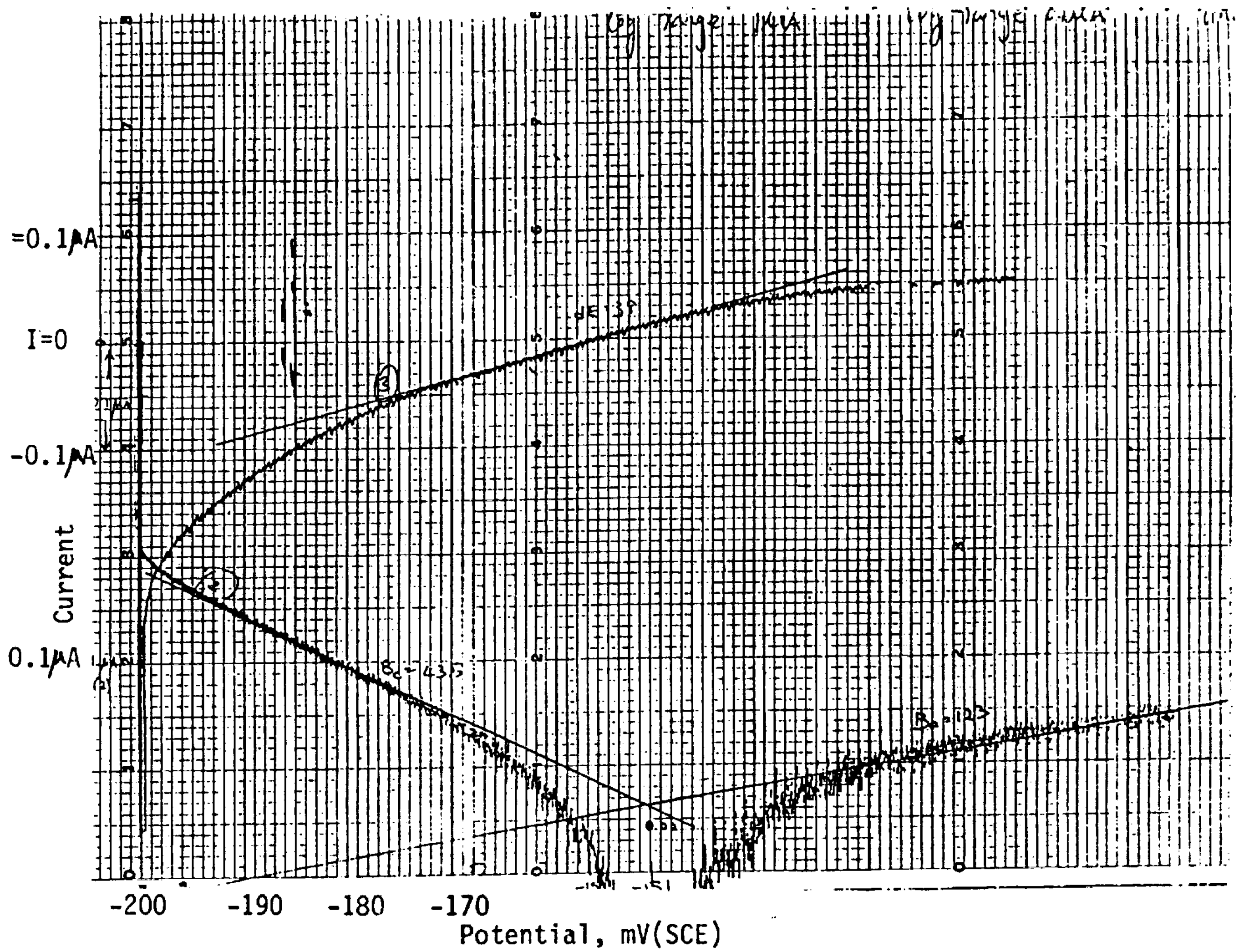

Figure 15 : Linear and log polarization plots for Al-TF on the Stage II five electrode sensor in immersion testing in tap water. First test. External calomel ref. electrode Au-TF counter electrode
Linear: X-axis: 1 inch = 10 mV (SCE); Starting potl. =-200 mV
Log.: 2 inch = 1 decade rise in I; 0.1 µA at 2 inch location. starting potl. = -200 mV.
Y-axis(linear): 1 inch = 0.1 µA.

Table VIII: Electrochemical corrosion parameters of Al and Cu thin films individually and in coupled modes in fog test with tap water fog.

Specimen	Aluminum TF				Copper TF				Al-Cu TFs coupled			
No. of cycle	E_{corr} (mV, Ag-TF)	R_p^* ($.cm^2$) ($x10^4$)	I_{corr} ($A.cm^{-2}$) extr.	I_{corr} calc.	E_{corr} (mV, Ag-TF)	R_p^* ($.cm^2$) ($x10^4$)	I_{corr} ($A.cm^{-2}$) extr.	I_{corr} calc.	E_{corr} (mV, Ag-TF)	R_p^* ($.cm^2$) ($x10^4$)	I_{corr} ($A.cm^{-2}$) extr.	I_{corr} calc.
1	-143	69	0.027	0.045	-98	76	0.022	0.040	-110	35	0.020	0.024
2	-113	34	0.03	0.09	-130	13	0.033	0.214	-120	14	0.024	0.067
5	-87	43	0.011	0.110	-114	34	0.013	0.134	-113	23	0.075	0.076
10	-86	37	0.03	0.05	-90	36	0.042	0.084	-102	44	0.054	0.334
21	-99	11	0.06	0.06	=102	7	0.09	0.208	-86	7.5	0.108	0.138
24	-114	10.8	0.12	0.114	-92	4	0.11	0.247	-91	4	0.038	0.048
29	-108	25	0.083	0.04	-96	1.5	0.11	0.457	-92	5.5	0.194	0.169
35	-91	2.3	0.054	0.705	-93	8.8	0.038	0.142	-93	5.5	0.065	0.178
46	-101	12	0.05	0.057	-101	4	0.084	0.168	-100	2.2	0.151	0.222
50	-101	12	0.15	0.163	-97	6.5	0.187	0.315	-92	4	0.13	0.19

As in immersion the corrosion potential of the couple seems to remain nearly stable around -100 mV. However, the potential in several instances is higher than the potential of the metal with the higher potential. In cycle # 21, the potential of the couple is -86 mV, which is higher than the potential of Al-TF, -99 mV, in cycle # 29, it is -92 mV, higher than -96 mV of Cu-TF, in the 50th cycle it is -92 mV, higher than the -97 mV value of Cu-TF, etc. The corrosion potential of the couple is also lower in one instance than the lowest potential of the two members in the couple. This is in cycle # 10 when the potential of the couple is -102 mV, below the lower potential of -90 mV of Cu-TF. Overall it is seen that the corrosion potential of the couple follows that of the higher potential metal or the one which shows higher corrosion rates, in this case the Cu-TF.

Overall it can be stated that the results obtained to date indicate the following:

1. Al-TF protects itself by passivating in milder electrolytes. It corrodes in chloride-containing electrolytes and condensates.
2. Compared to Al-TF, the Cu-TF corrodes more uniformly and does not passivate in electrolytes that would appear in the atmosphere. So copper is a much better sensor element.
3. Cu-TF corrodes more than the Al-TF in similar environments.
4. When combined together and tested against the Au-TF counter electrode, the behavior of the couple is dictated by the Cu-TF electrode that corrodes more, although its potential is higher than that of the Al-TF electrode. The net corrosion current seems to follow that of the higher corrosion rate of Cu-TF. The Al-TF would seem to corrode very little in the couple.
5. Wet-dry cyclic conditions vastly determine the formation of the electrolyte film on the sensor complex as well as its wetting. Complete removal of the condensed moisture film is not indicated, except in cases of direct sun hit, where the surface would be heated appreciably.
6. Considerable corrosion is possible during the drying period, though the current density could be much lower.

5.0 CONCLUSIONS AND SUMMARY

Work has been carried out on techniques for evaporation and sputtering of selected materials on selected substrates to obtain thin film coatings to produce specimen atmospheric corrosion microsensors. Two designs of Stage I and Stage II microsensors have been devised and characterization and evaluation of these for atmospheric corrosion conditions in selected environments have been carried out for electrochemical behavior and selected fog testing. A modern sputtering equipment PELCO SC5 unit has been procured and is to be further utilized in carrying out the processing of thin films for different designs of the corrosion sensor thin films. Detailed analyses of electroechemical corrosion effects have then to be further analyzed.

APPENDIX

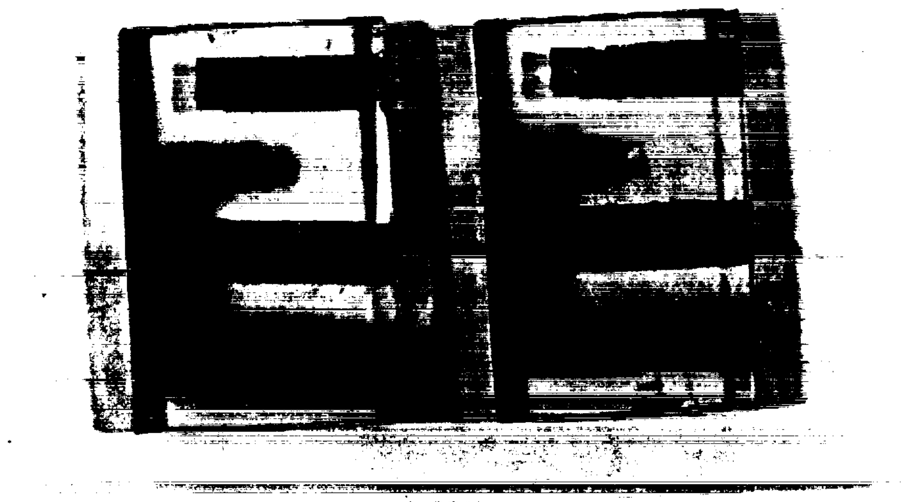

STAGE I MICROSENSORS

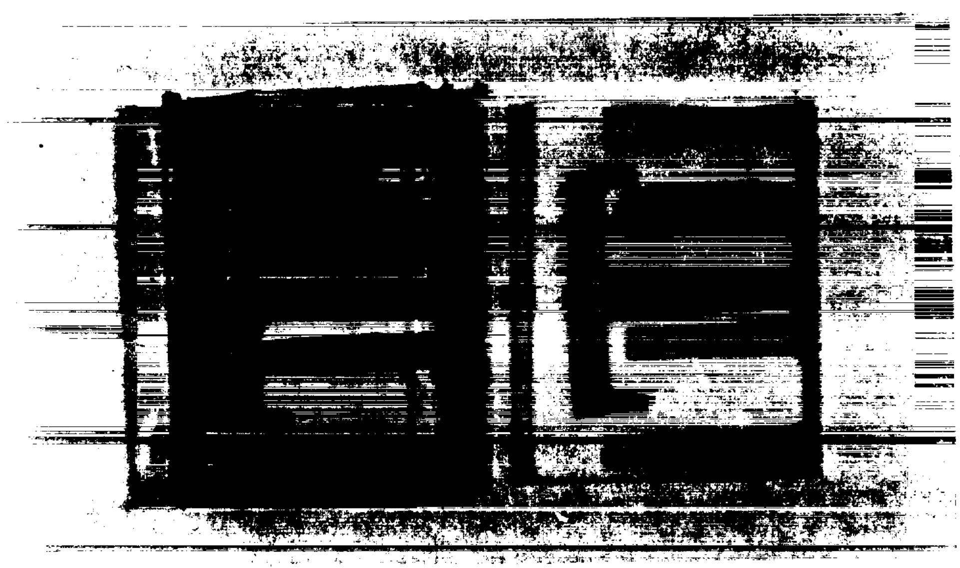

STAGE II MICROSENSORS

Figure A1: Photographs of Stage I and Stage II microsensors as shown under fabrication. The photograph of Stage I microsensor on glass substrates show some shadow of the electrode elements at the edges. No shadow is seen in case of alumina substrates for stage II microsensors.

FIGURE A2: Photograph of research team members shown involved in the study and development of the atmospheric microsensor project.

PRINCIPAL INVESTIGATOR
DR. RAVINDER M. DIWAN

CO-PRINCIPAL INVESTIGATOR
DR. A. RAMAN

CO-PRINCIPAL INVESTIGATOR
DR. P. K. BHATTACHARYA

Figure A3: Research Project Team Members showing Principal Investigator and Co-Principal Investigators.

MR. MANOJ CHHABRA
GRADUATE STUDENT

MS. FELESHA ROBERTSON
SENIOR M. E. STUDENT

MR. CHIN-SUING TEO
SENIOR CH.E.STUDENT

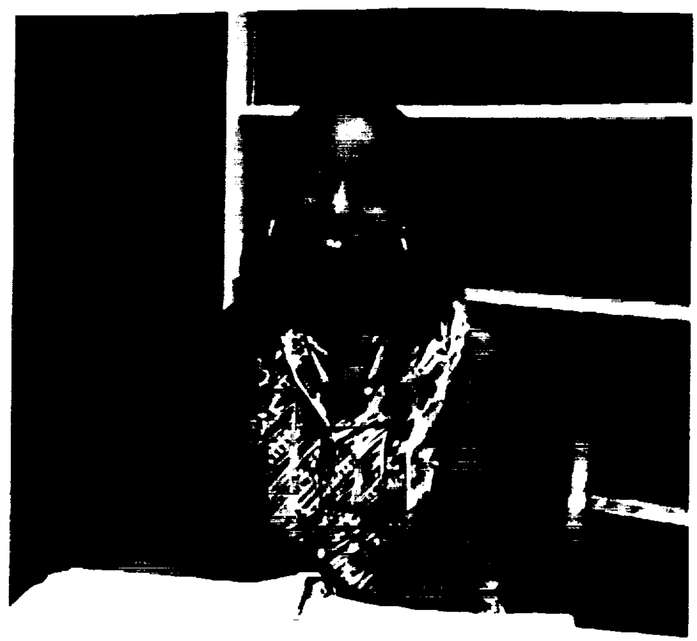

MS. LORANN JONES
SENIOR E.E. STUDENT

Figure A4: Research Project Student assistants showing graduate student and Undergraduate students.

MR. WENSEN LI

GRADUATE STUDENT

Figure A5: Research Project Student assistant conducting corrosion testing.

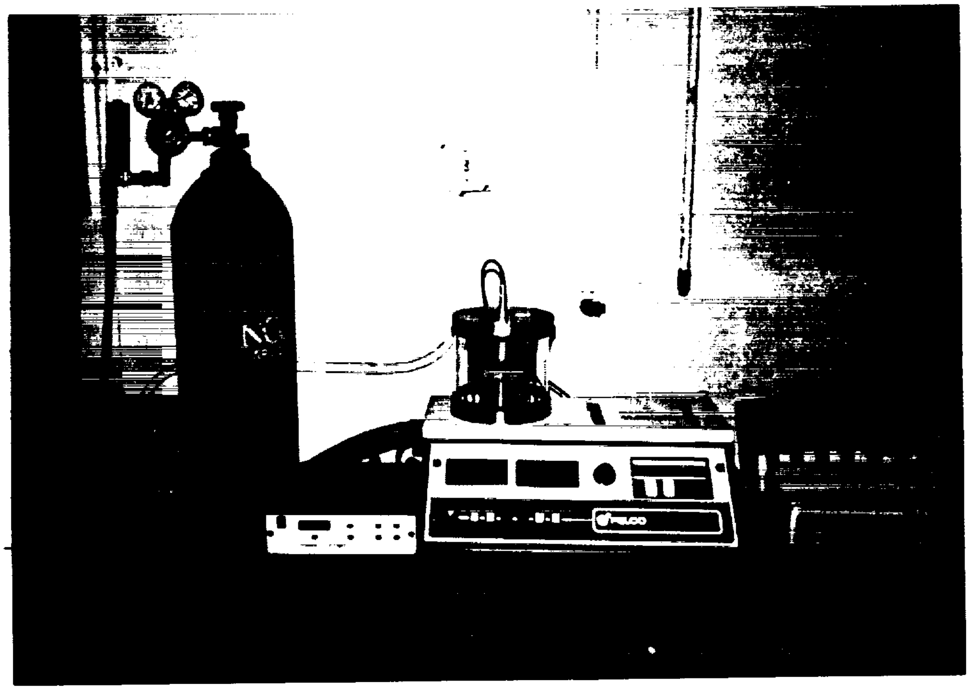

Figure A6: PELCO PC5 Sputter Coating unit procured for thin film coating work.

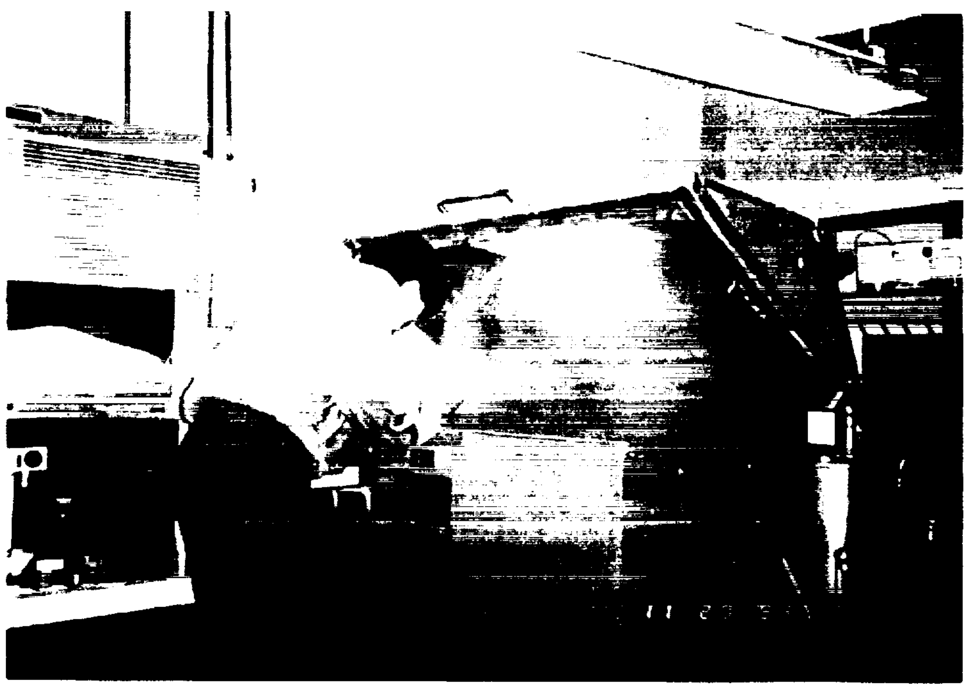

Figure A7: Corrosion Chamber Fog Testing.